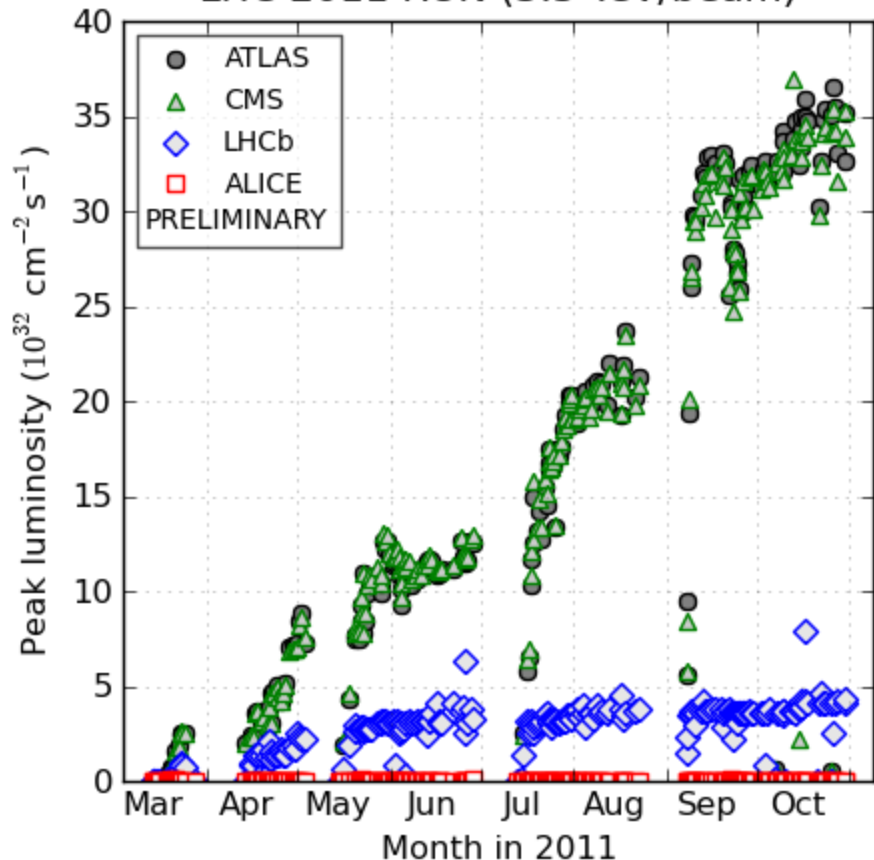


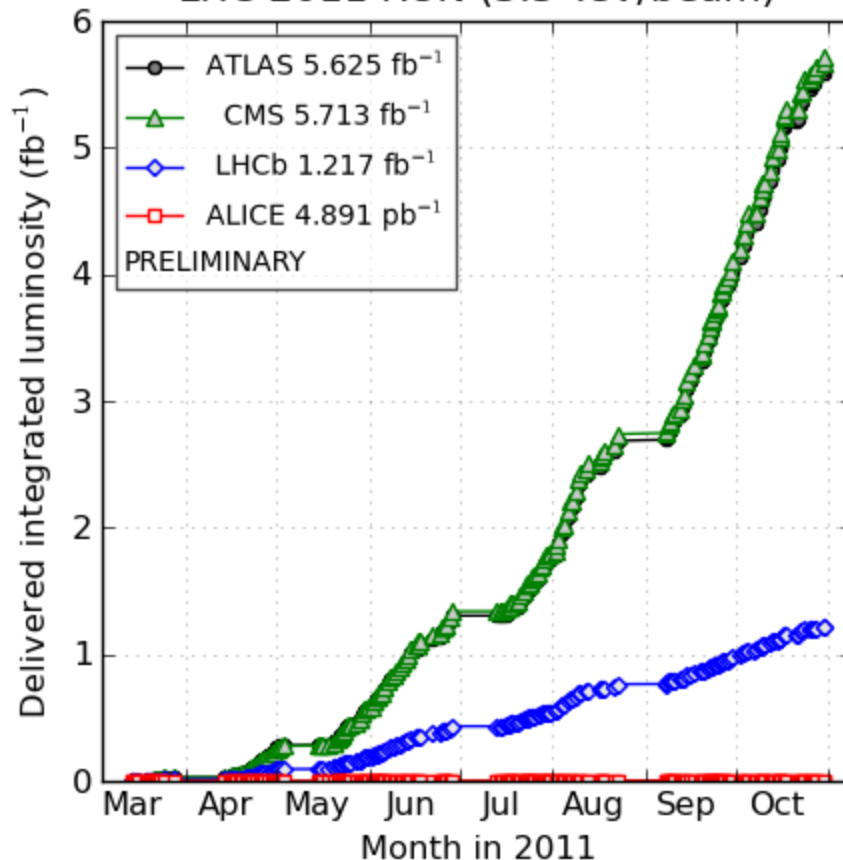
LHC Luminosity Plots for the 2011 Proton Run

LHC 2011 RUN (3.5 TeV/beam)



(generated 2011-11-20 20:22 including fill 2267)

LHC 2011 RUN (3.5 TeV/beam)

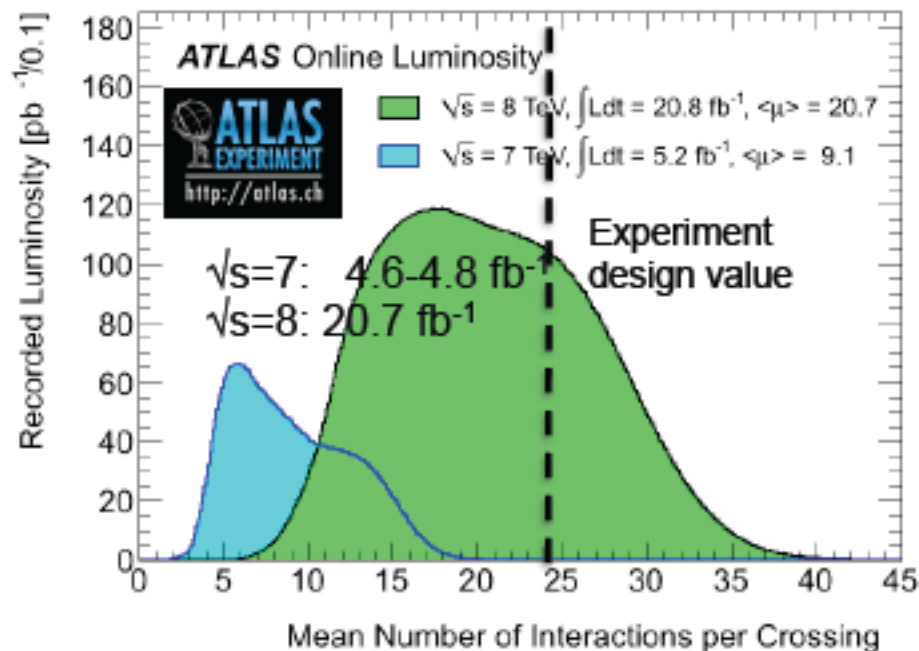
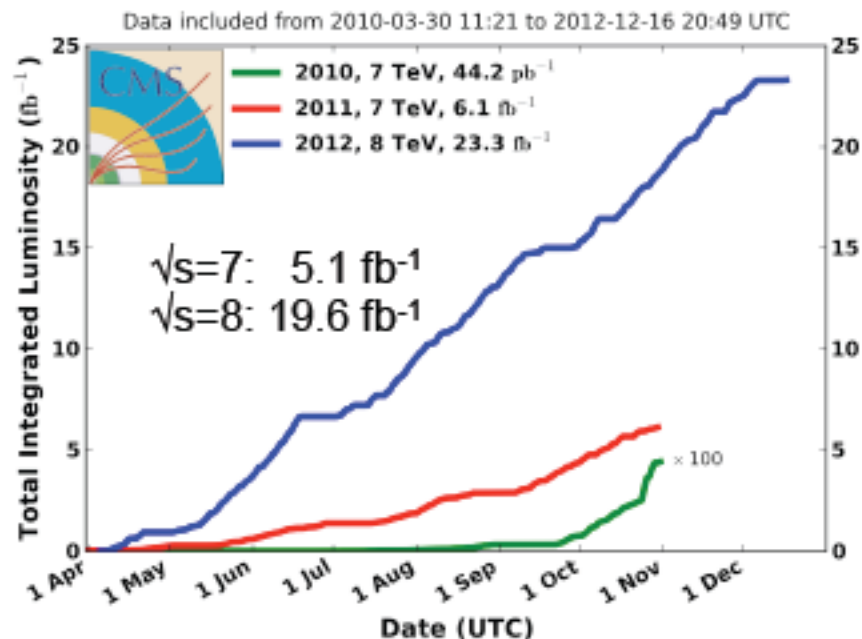


(generated 2011-11-20 20:22 including fill 2267)

Ziel: peak Lumi $L=10^{34} \text{ cm}^{-2} \text{ s}^{-1}$

<http://lpc.web.cern.ch/lpc/lumiplots.htm>

CMS Integrated Luminosity, pp



Detectors at accelerators experiments

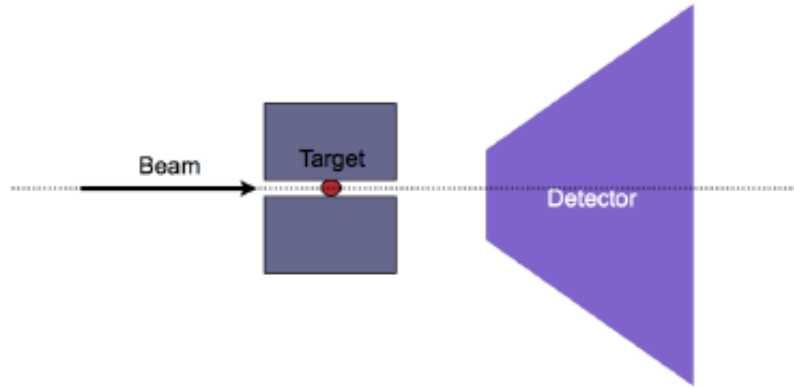


Figure 4.14: *Schematic view of an experimental setup for a fixed target experiment.*

Bestimmung von
-Raumkoordinaten und
Zeiten der
Endzustände
-Impulse der Teilchen
-Energy der Teilchen
-Art der Teilchen (PID)

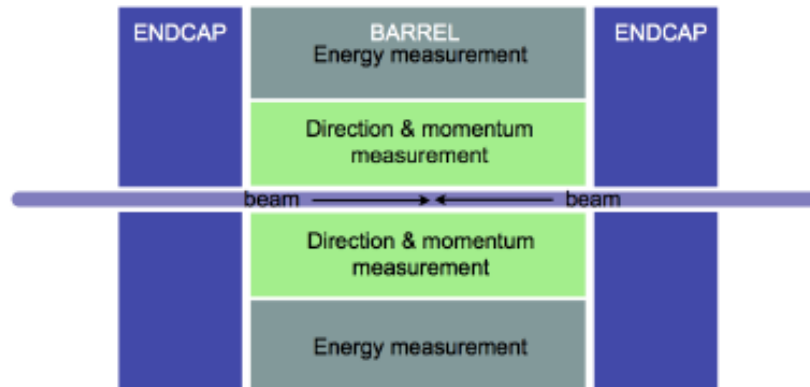


Figure 4.15: *Schematic view of a detector for colliding beam experiments.*

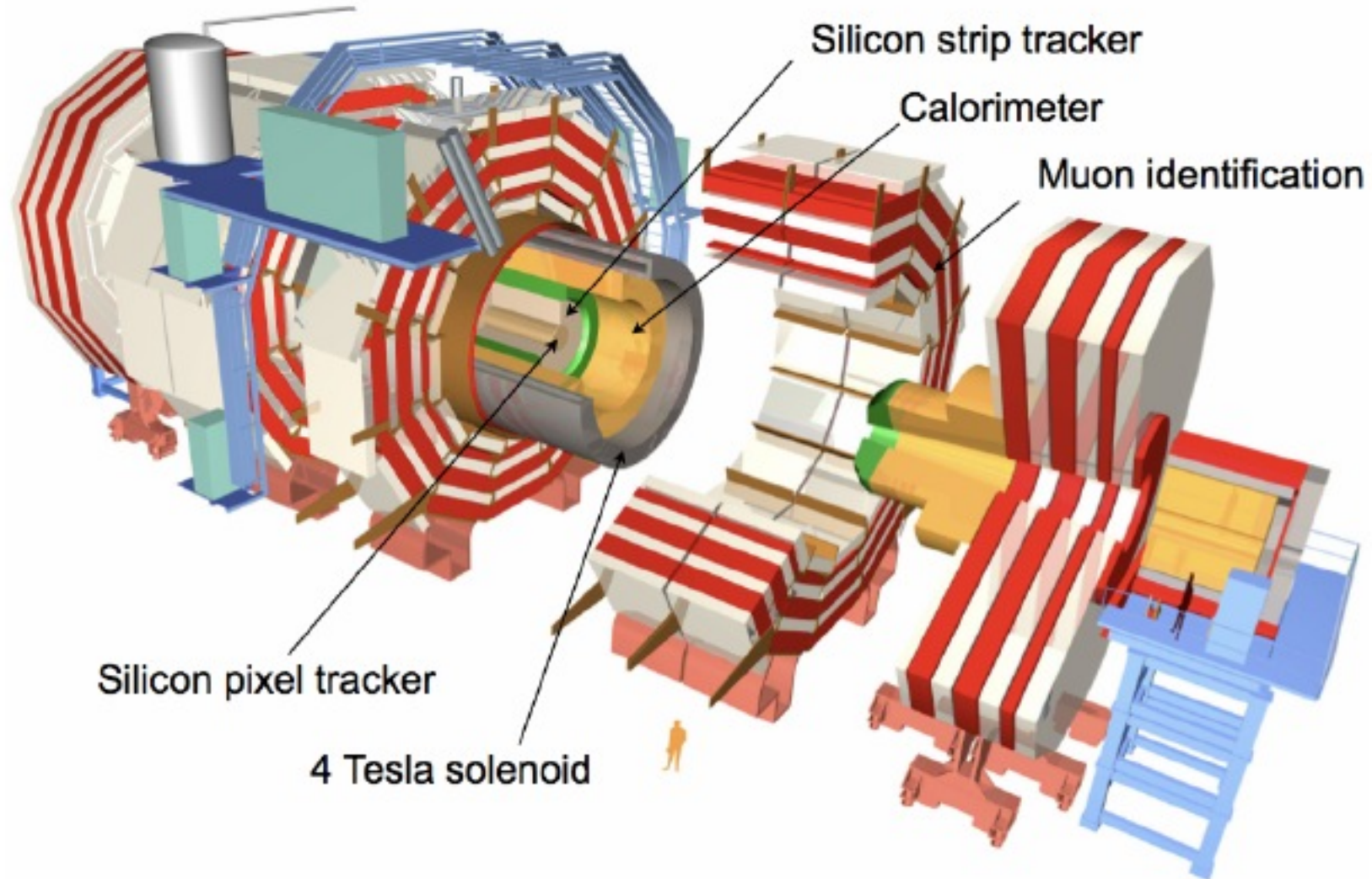


Figure 4.16: *The CMS experiment at the LHC.*

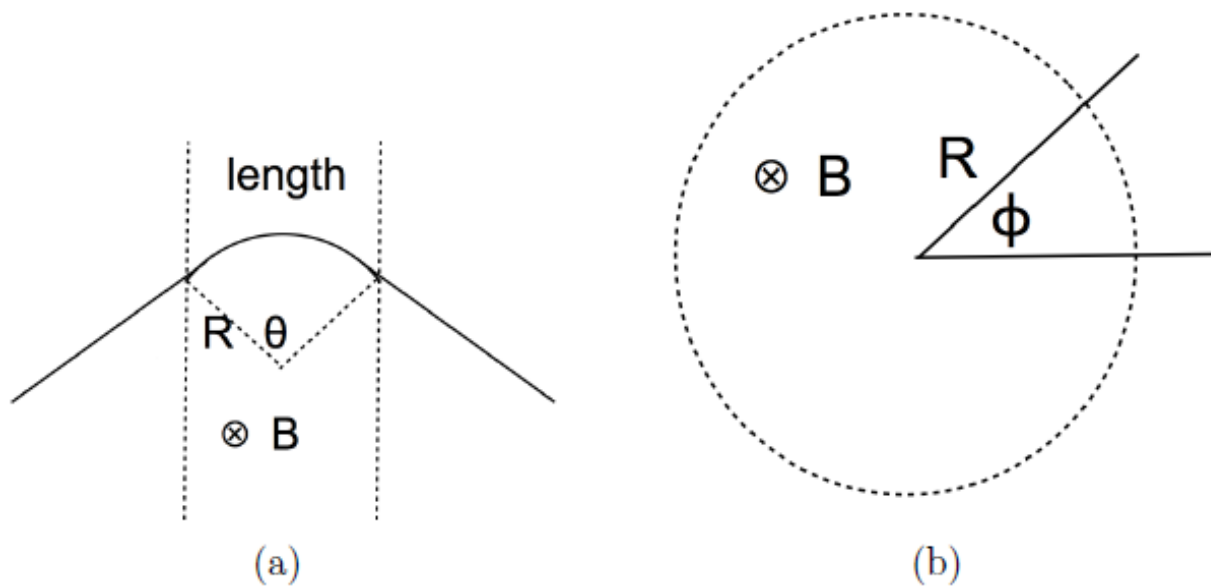


Figure 4.17: *Momentum measurement in collider experiments using a magnetic field.* The magnetic field is parallel to the beams (orthogonal to the page).

$$p = 0.3BR$$

$$\text{length} = l = 2R \sin\left(\frac{\theta}{2}\right) \sim R\theta$$

$$\Rightarrow \theta = \frac{\text{length}}{R} = \frac{0.3Bl}{p}$$

$$\Rightarrow p = \frac{0.3Bl}{\theta}.$$

Transversaler u. longitudinaler Impuls

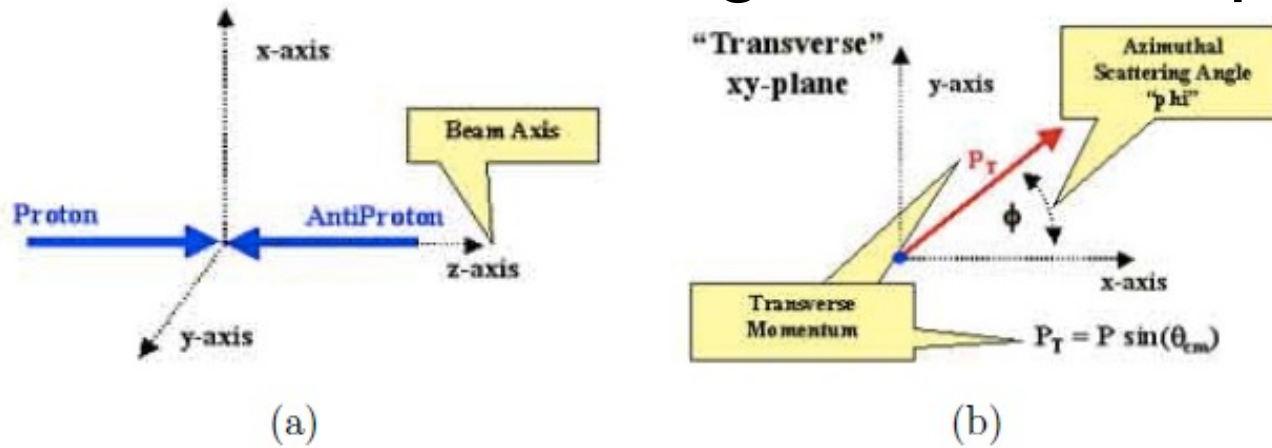


Figure 4.18: Axes labelling conventions (a) and definition of transverse momentum (b).
 S

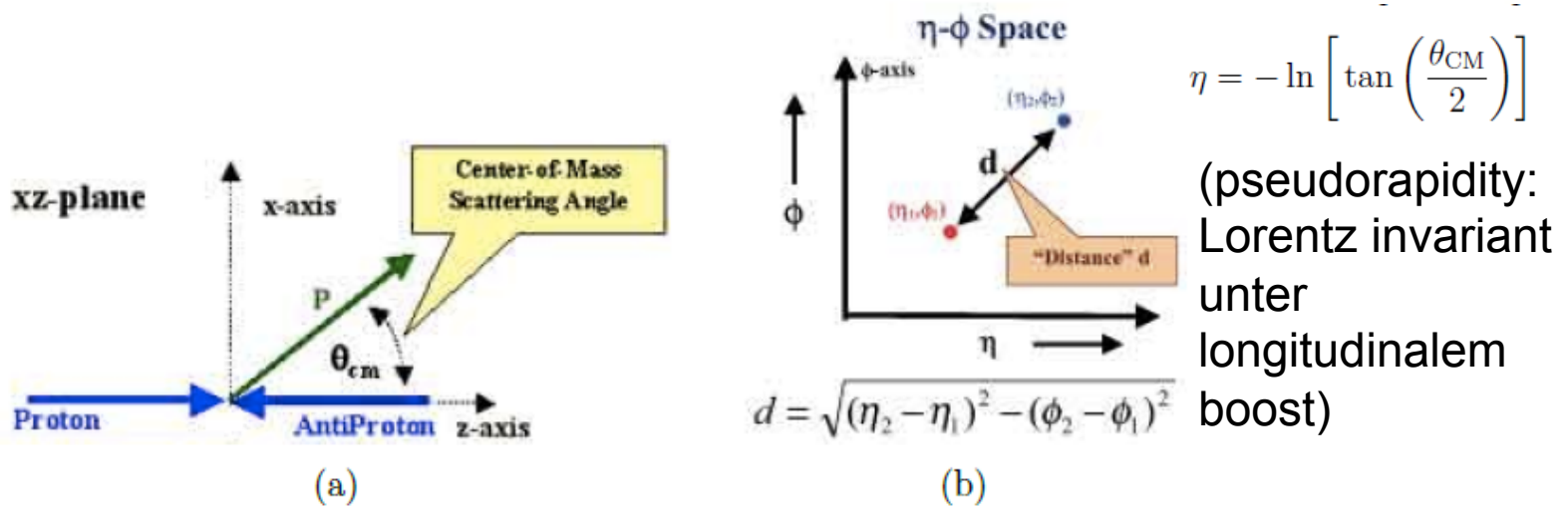


Figure 4.19: Definition of the longitudinal scattering angle θ_{CM} (a) and definition of particle distance in the η - ϕ plane (b). Source: [10].

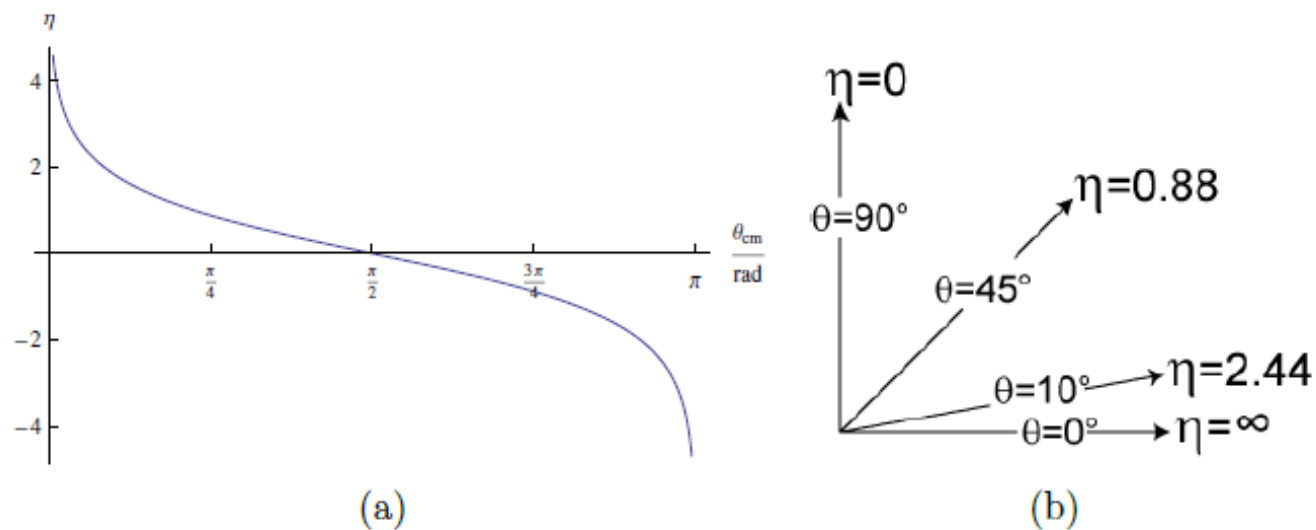
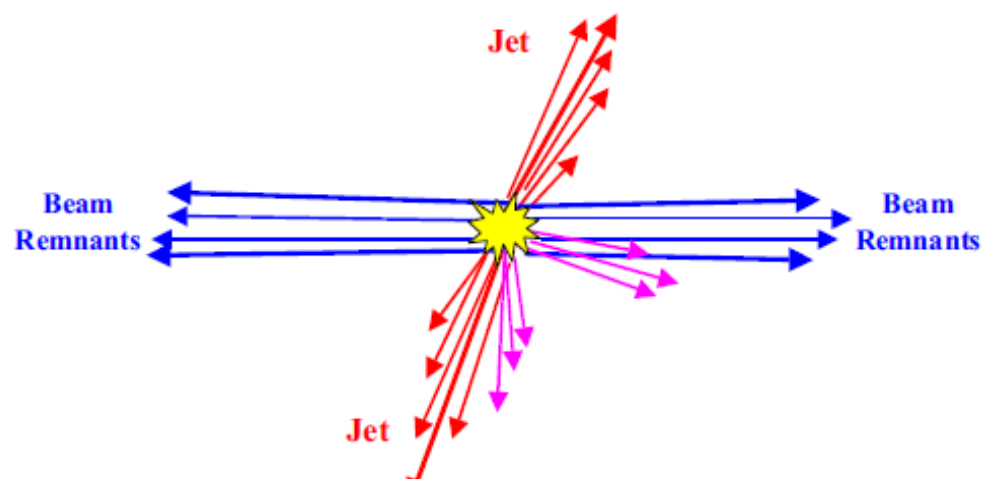


Figure 4.20: Pseudorapidity as a function of θ_{CM} (a) and pseudorapidity for various values of θ_{CM} (b). Source (b): [11].



Kein transversaler Impuls vor Streuprozess \Rightarrow Gesamt Transversalimpuls der final state Teilchen muss identisch null sein

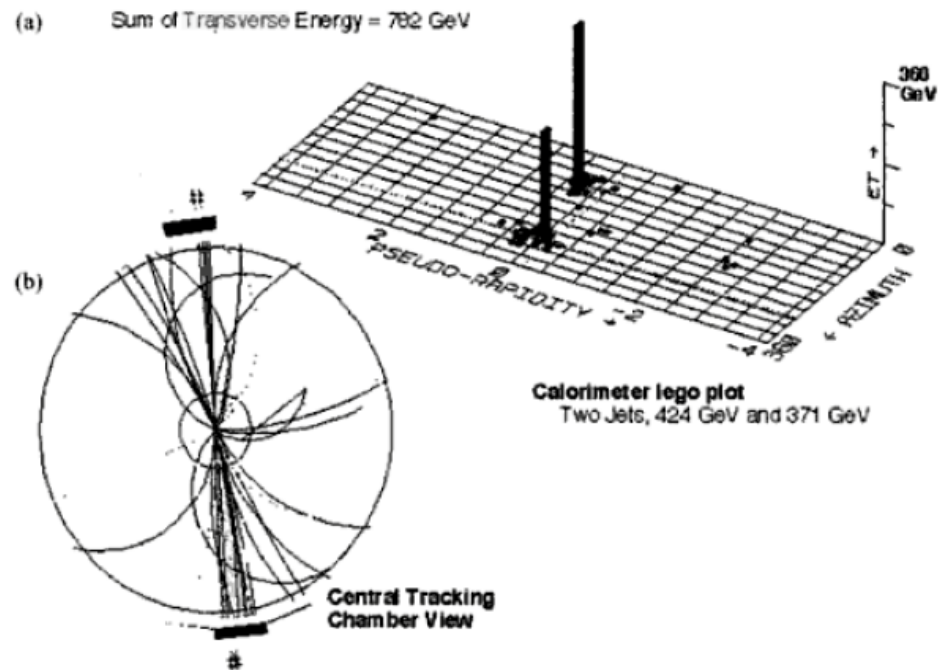


Figure 4.22: Two jet event, reconstructed in the tracking chamber (b) and calorimeter signals (a) of the $D\bar{O}$ experiment.

Missing mass method

A collision is characterized by an initial total energy and momentum $(E_{\text{in}}, \vec{p}_{\text{in}})$. In the final state we have n particles with total energy and momentum given by:

$$E = \sum_i^n E_i, \quad (4.10)$$

$$\vec{p} = \sum_i^n \vec{p}_i. \quad (4.11)$$

Sometimes an experiment may measure $E < E_{\text{in}}$ and $\vec{p} \neq \vec{p}_{\text{in}}$. In this case one or more particles have not been detected. Typically this happens with neutral particles, most often neutrinos, but also with neutrons, π^0 , or K_L^0 . The latter have a long lifetime and may decay outside the sensitive volume. To quantify this process, we introduce the concept of missing mass:

$$\text{missing mass} \times c^2 = \sqrt{(E_{\text{in}} - E)^2 - (\vec{p}_{\text{in}} - \vec{p})^2 c^2}. \quad (4.12)$$

The missing mass is measured for every collision and its spectrum is plotted. If the spectrum has a well-defined peak one particle has escaped our detector.

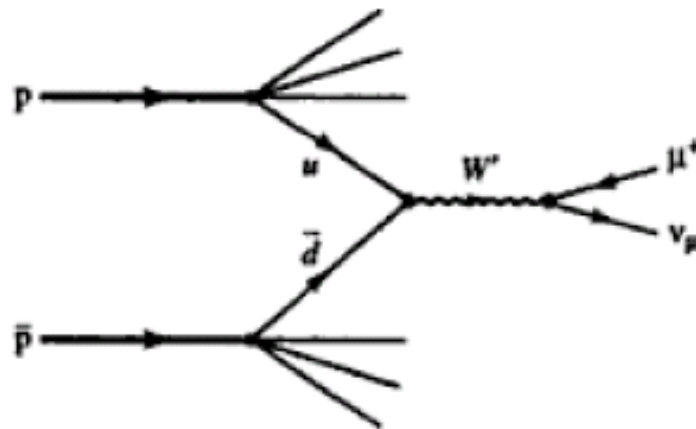


Figure 4.24: *Production and decay of a W^+ boson in a $p\bar{p}$ collision.*

Muon-Impuls wird gemessen, Neutrino entweicht Detektor
 Gesamtsumme des transversalen Impulses ist ungleich 0!
 Experimentelle Signatur: fehlender transversaler Impuls

Invariant mass method

The invariant mass is a characteristic of the total energy and momentum of an object or a system of objects that is the same in all frames of reference. When the system as a whole is at rest, the invariant mass is equal to the total energy of the system divided by c^2 . If the system is one particle, the invariant mass may also be called the rest mass:

$$m^2 c^4 = E^2 - \vec{p}^2 c^2.$$

For a system of N particles we have

$$W^2 c^4 = \left(\sum_i^N E_i \right)^2 - \left(\sum_i^N \vec{p}_i c \right)^2 \quad (4.13)$$

where W is the invariant mass of the decaying particle. For a particle of Mass M decaying into two particles, $M \rightarrow 1 + 2$, Eq. 4.13 becomes:

$$M^2 c^4 = (E_1 + E_2)^2 - (\vec{p}_1 + \vec{p}_2)^2 c^2 = m_1^2 c^4 + m_2^2 c^4 + 2(E_1 E_2 - \vec{p}_1 \cdot \vec{p}_2 c^2) = (p_1 + p_2)^2.$$

Invariante Masse: $\pi^0 \rightarrow \gamma\gamma$

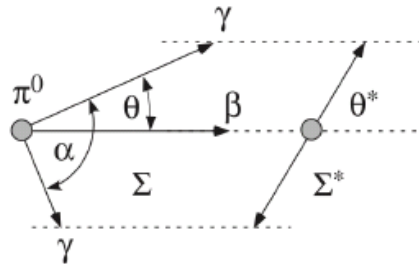


Figure 4.28: π^0 decay in two photons. Σ denotes the laboratory frame (left) and Σ^* denotes the pion rest frame (right). Source [8, p. 95].

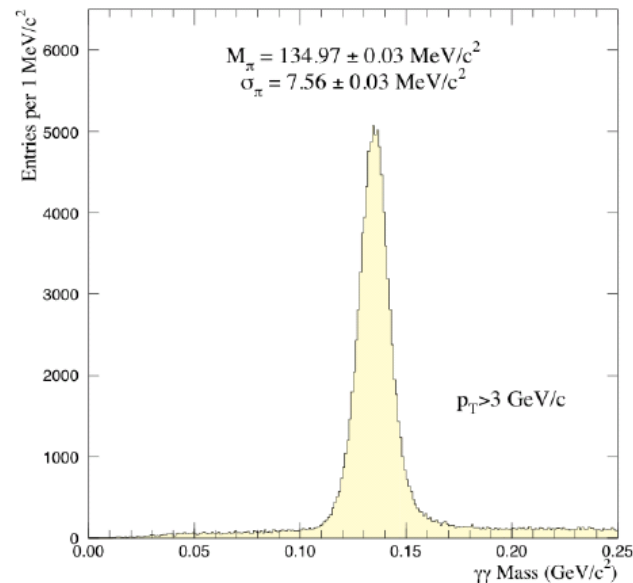
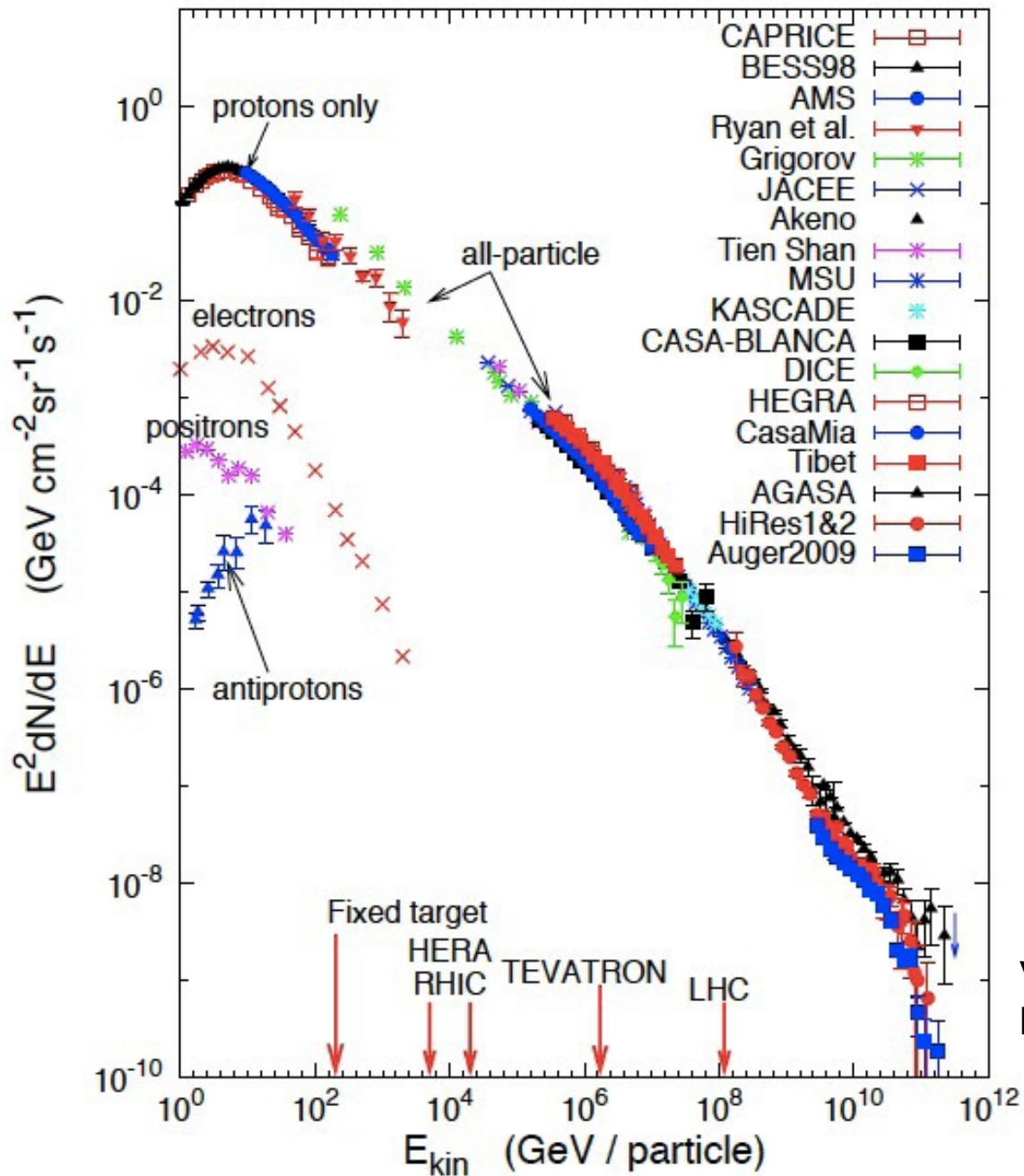


Figure 4.29: Invariant mass spectrum for photon pairs. The π^0 appears as a peak at the pion mass.

Energies and rates of the cosmic-ray particles



Vgl. mit collider korrigiert auf \sqrt{s}

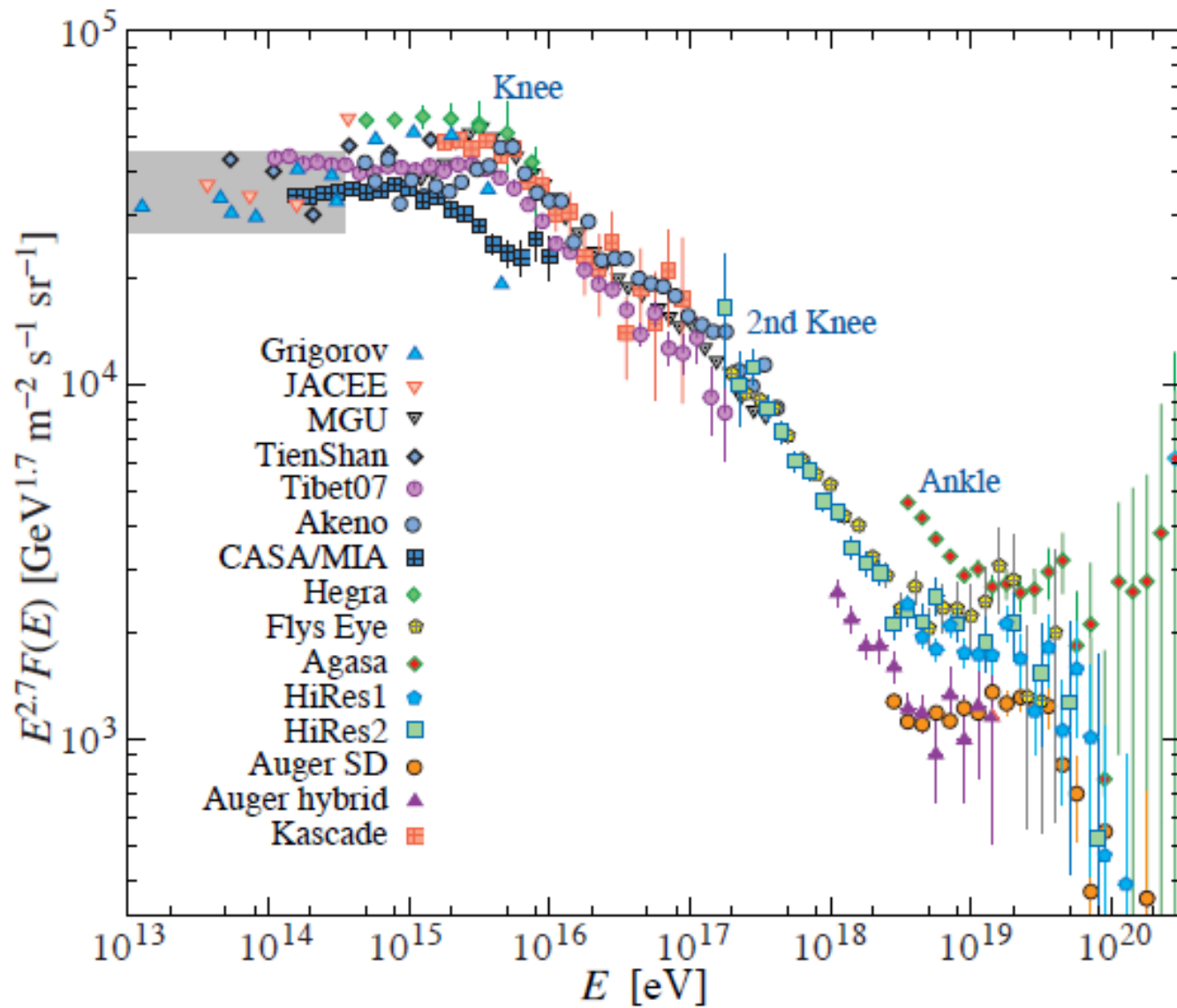
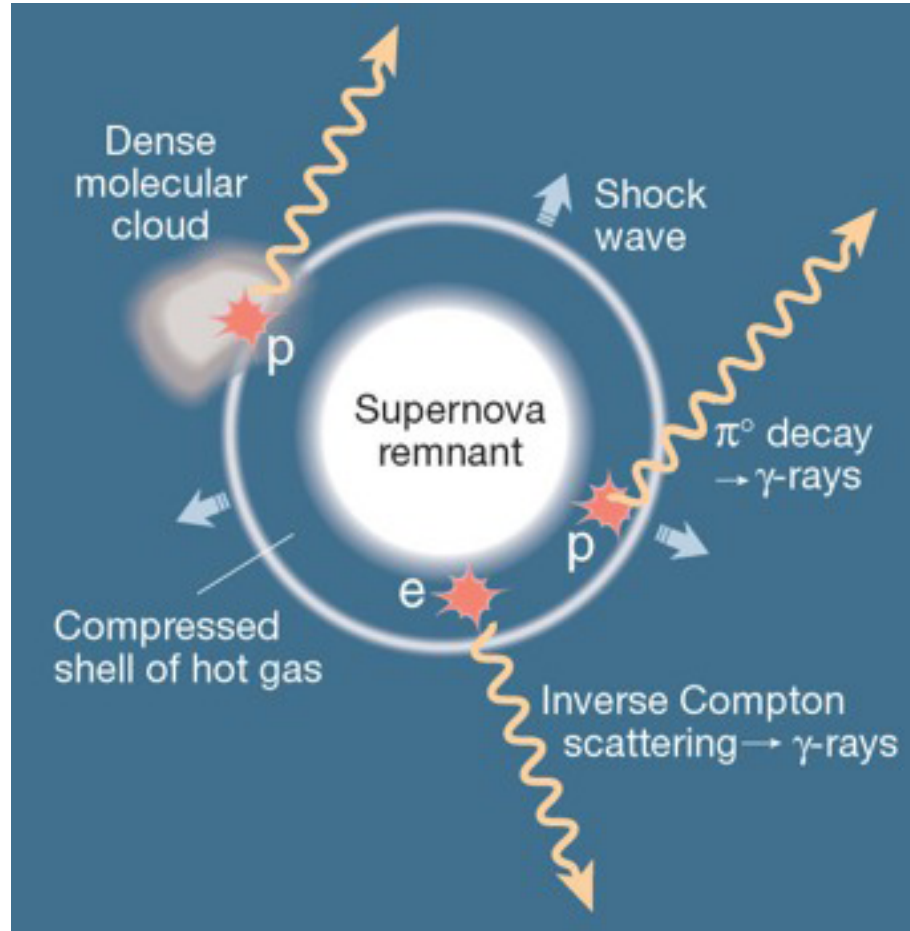
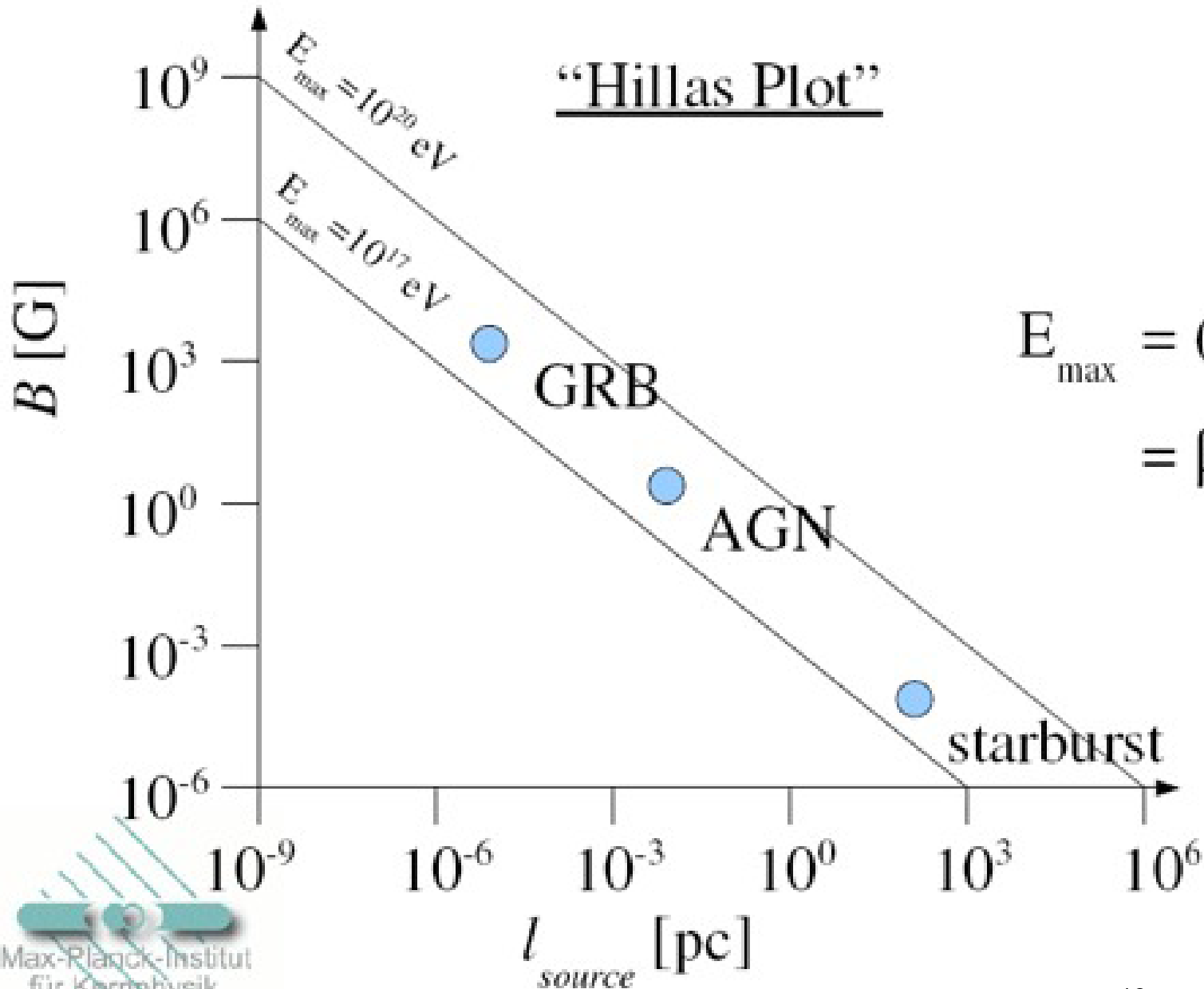


Figure 24.8: The all-particle spectrum from air shower measurements. The shaded area shows the range of the the direct cosmic ray spectrum measurements. See full-color version on color pages at end of book. T. Gaisser, T. Stanev in www.pdg.lbl.gov



Felix Aharonian, Nature **416**, 797-798, 2002



$$E_{max} = (Bc)R_{Larmor}$$

$$= \beta_{sh} (Bc) l_{source}$$

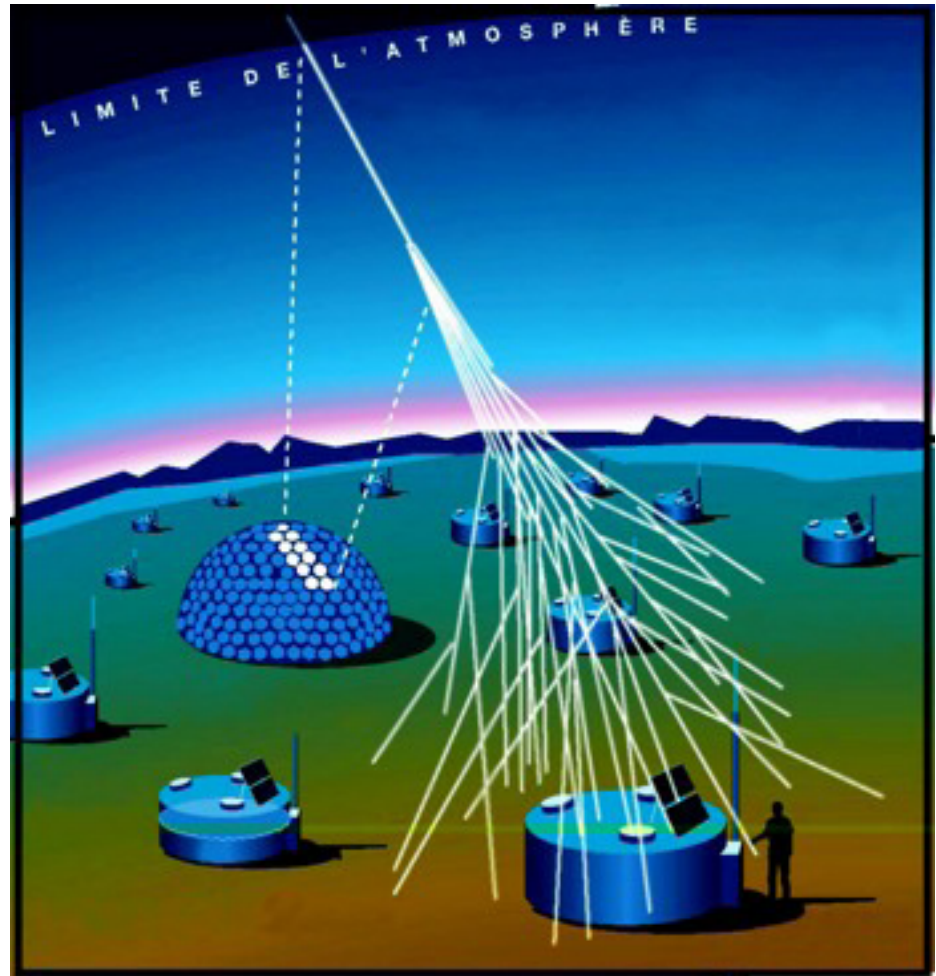
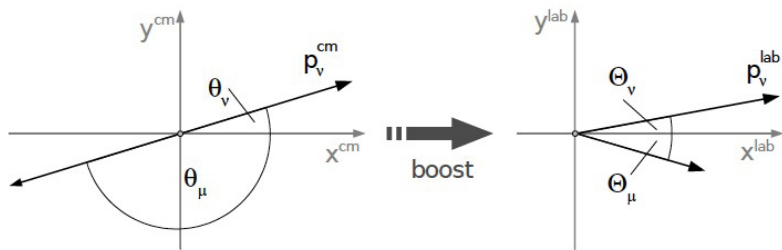
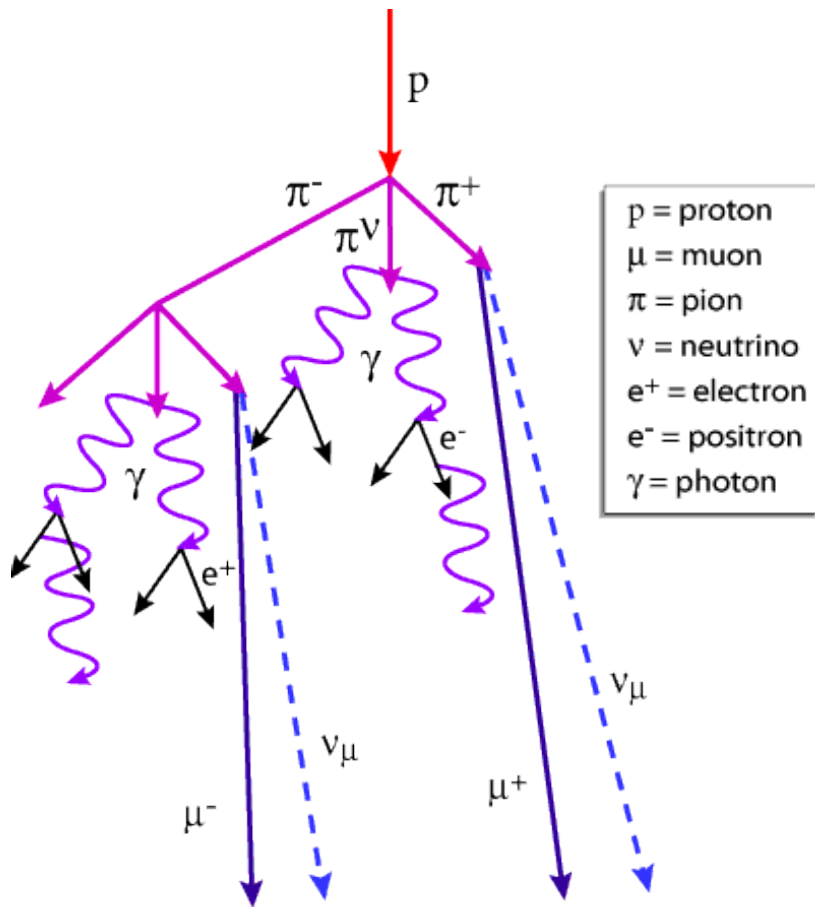


Figure 2.4: Two body decay of the parent meson into muon and neutrino. - The left figure displays the back-to-back kinematics in the meson center of mass (cm) frame. The right figure shows the momenta after Lorentz transformation into the laboratory frame.

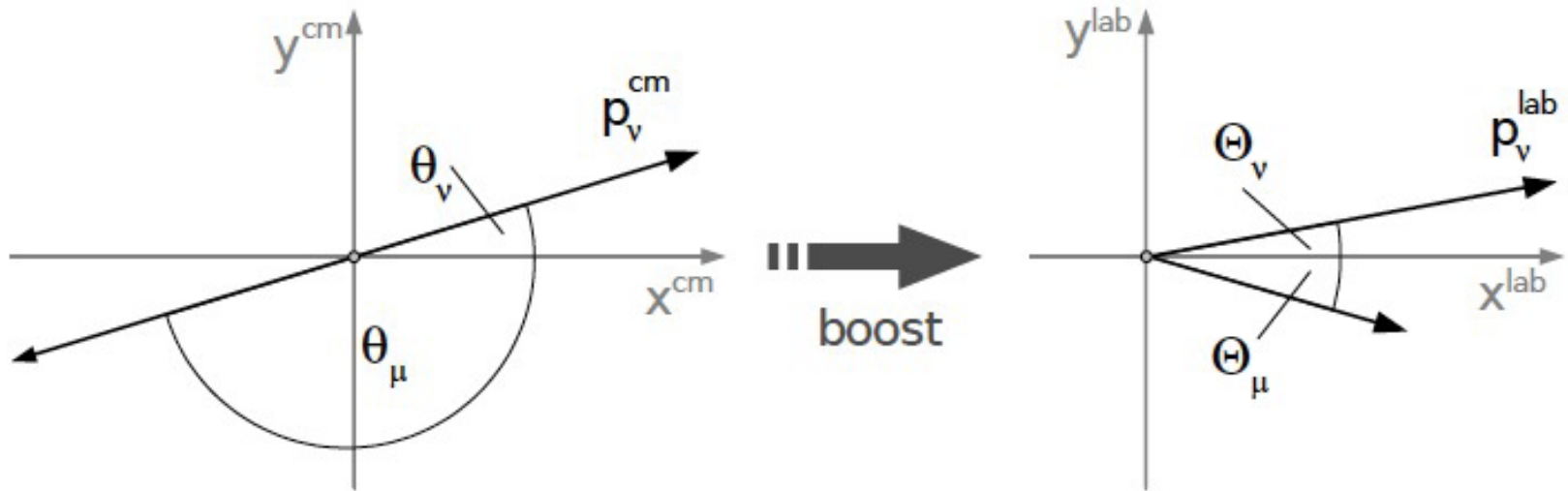


Figure 2.4: Two body decay of the parent meson into muon and neutrino. - The left figure displays the back-to-back kinematics in the meson center of mass (cm) frame. The right figure shows the momenta after Lorentz transformation into the laboratory frame.

$$E_\nu = \gamma E_\nu^{cm} + \beta \gamma p_{x\nu}^{cm}$$

$$p_{x\nu}^{cm} = |p^{cm}| \cos \theta_\nu \quad \text{and}$$

$$E_\mu = \gamma E_\mu^{cm} + \beta \gamma p_{x\mu}^{cm},$$

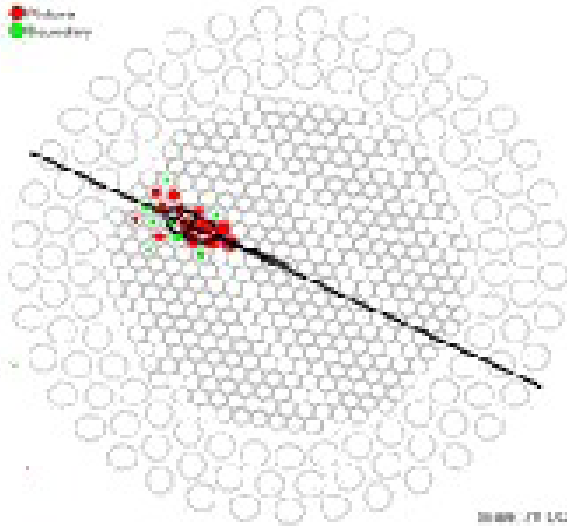
$$p_{x\mu}^{cm} = |p^{cm}| \cos(\theta_\nu - \pi) = -|p^{cm}| \cos \theta_\nu,$$

$$E_\nu = \gamma |p^{cm}| (1 + \cos \theta_\nu) \quad \text{and}$$

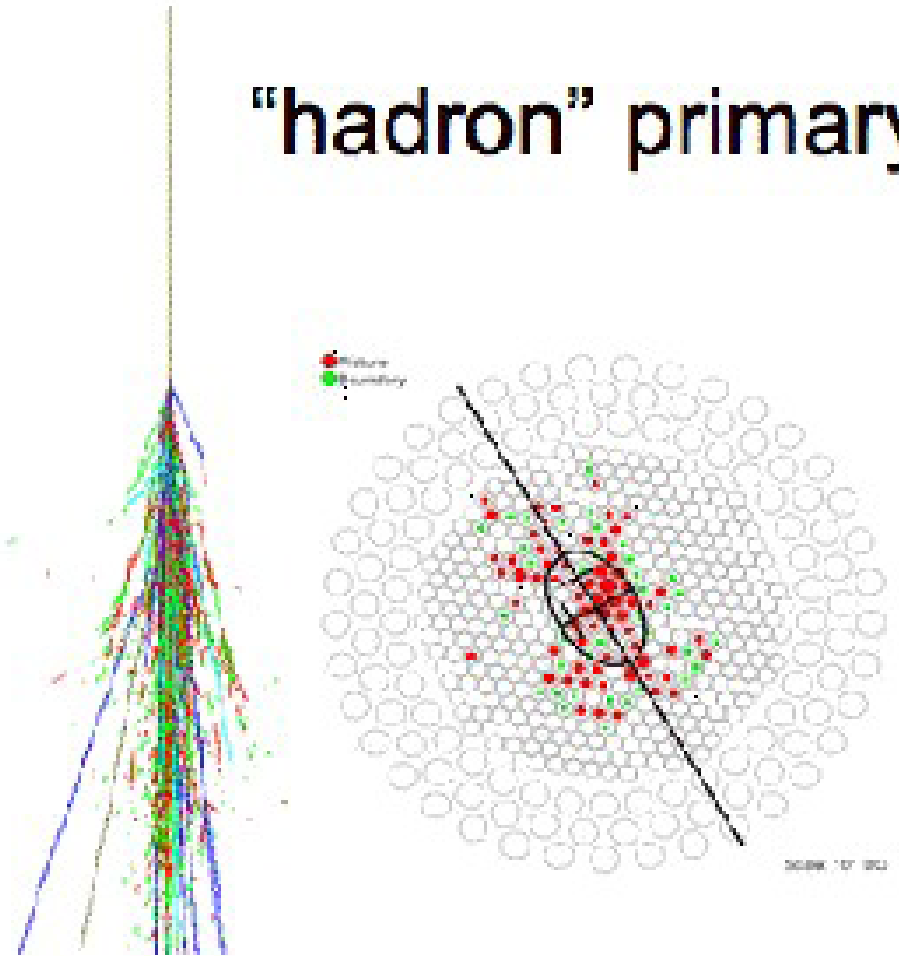
$$r_i = m_\mu^2 / m_i^2$$

$$E_\mu = \gamma |p^{cm}| \left(\frac{1 + r_i}{1 - r_i} - \cos \theta_\nu \right).$$

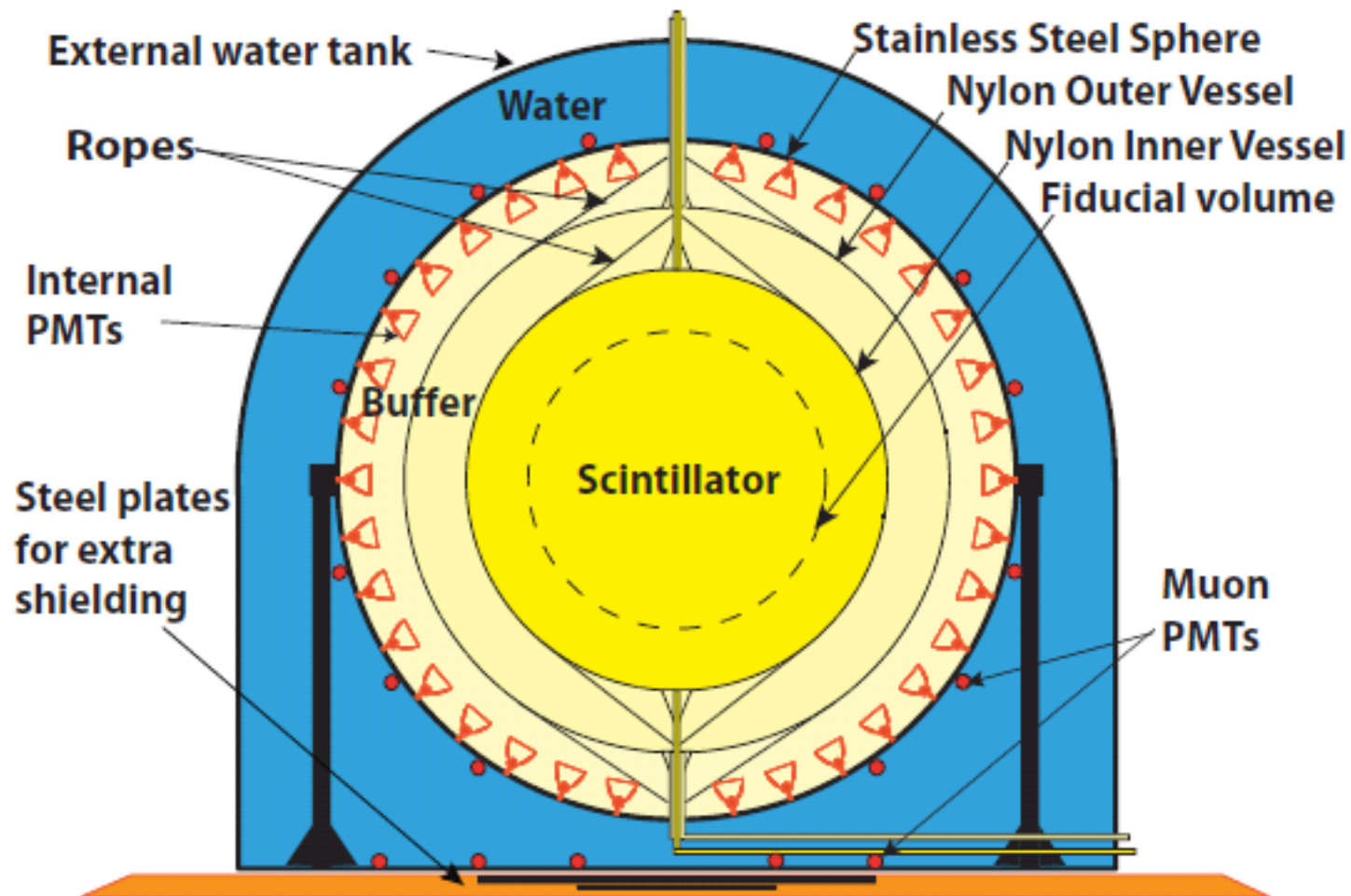
γ primary



"hadron" primary



Borexino Detector



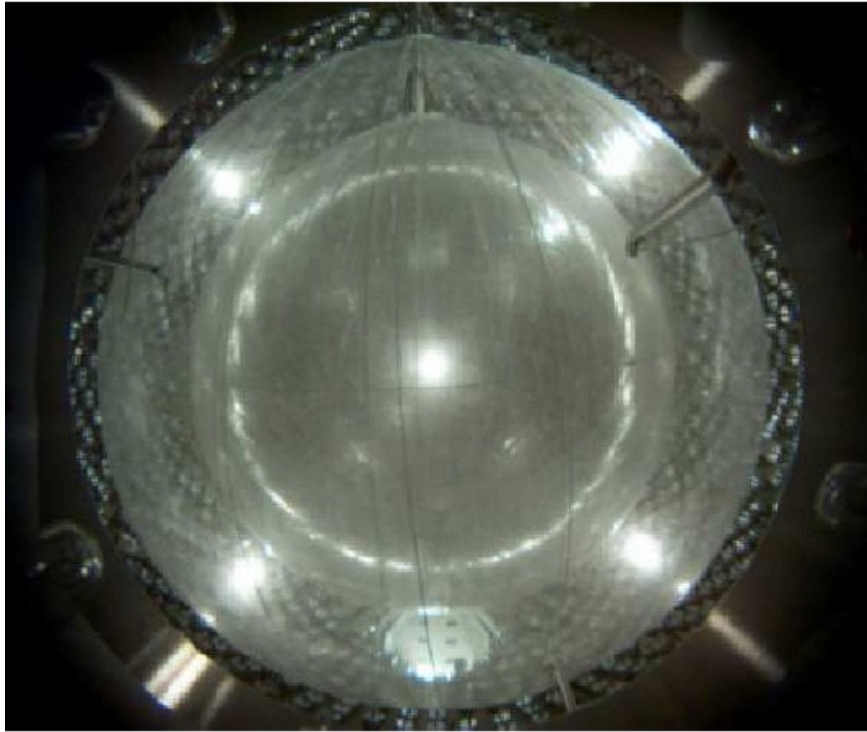


Fig. 2. The Inner and Outer Nylon Vessels installed and inflated with nitrogen in the Stainless Steel Sphere.

a buffer is convenient because it matches both the

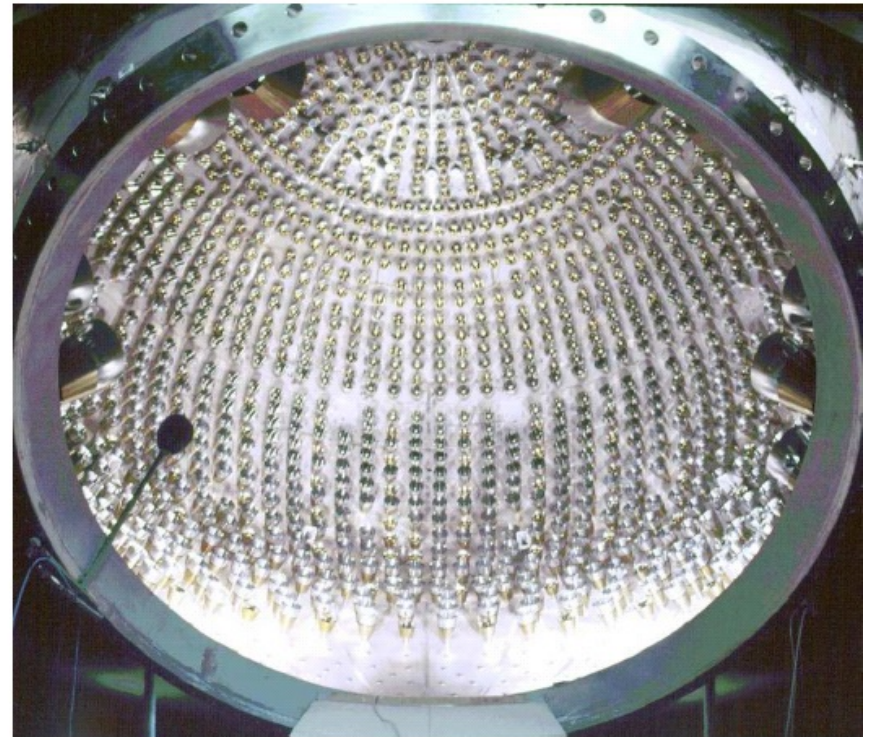


Fig. 3. Inner surface of the Stainless Steel Sphere. The picture is taken from the main SSS door, and shows the internal surface of the sphere with PMTs evenly mounted inside. The total number of PMTs is 2212.

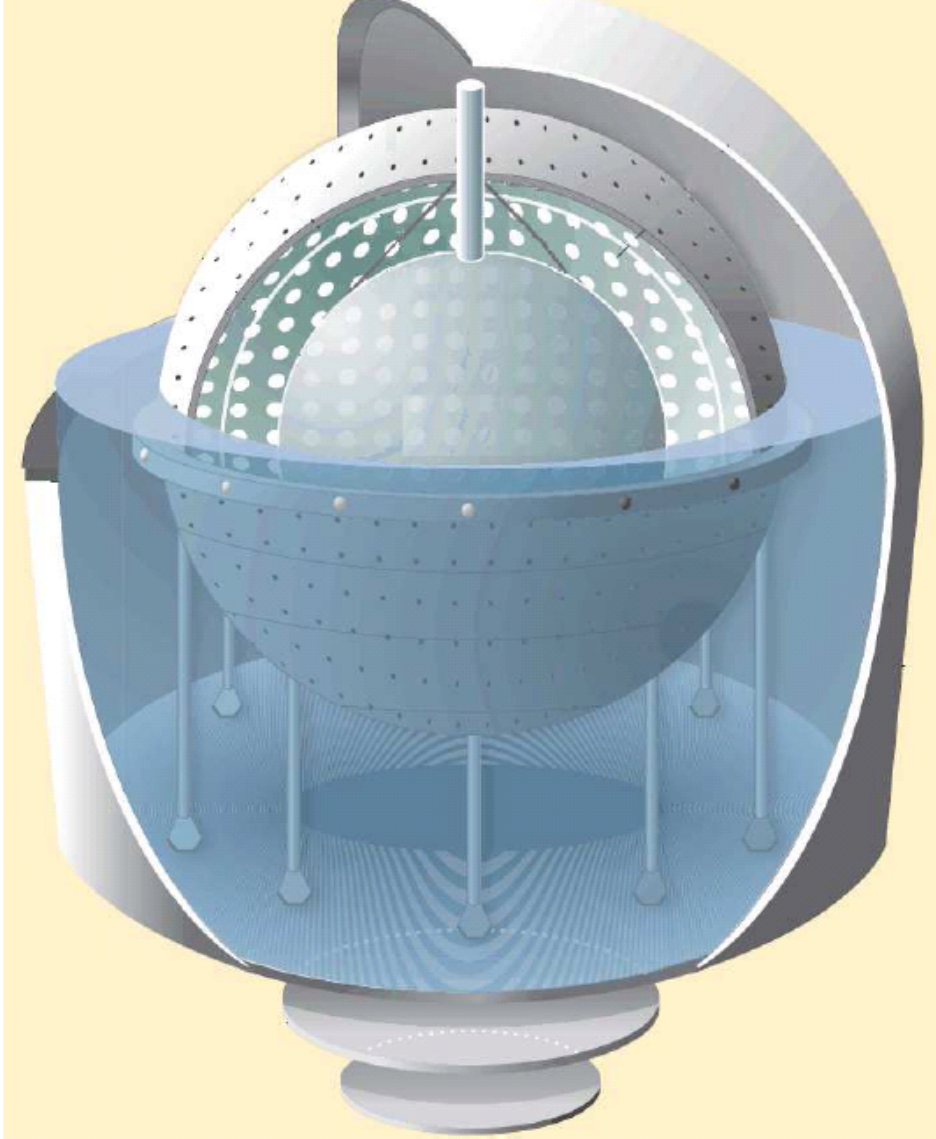


Fig. 4. A pictorial drawing of the Borexino detector. Inside the Water Tank, the Stainless Steel Sphere is supported by 20 steel legs. Within the sphere, the drawings shows some PMTs (white full circles) and the Inner and Outer Nylon Vessels. The steel plates beneath the tank improve the shielding against radiation from the rock.



Fig. 5. The inner surface of the Water Tank covered with a layer of Tyvek. The Tyvek sheets improve light collection in the Outer Detector by reflecting the photons back into the water.

gether with the low absorption of the scintillator⁶

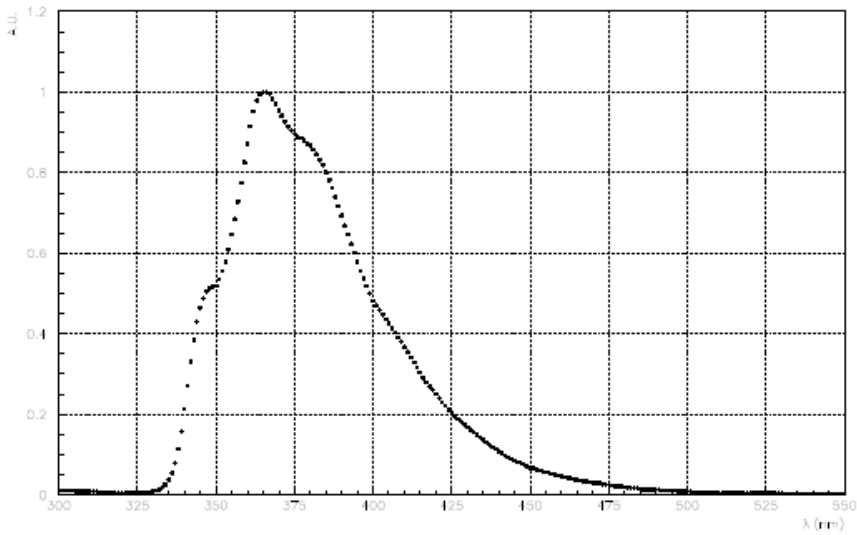


Fig. 6. Emission spectrum of the PC+PPO mixture used in Borexino

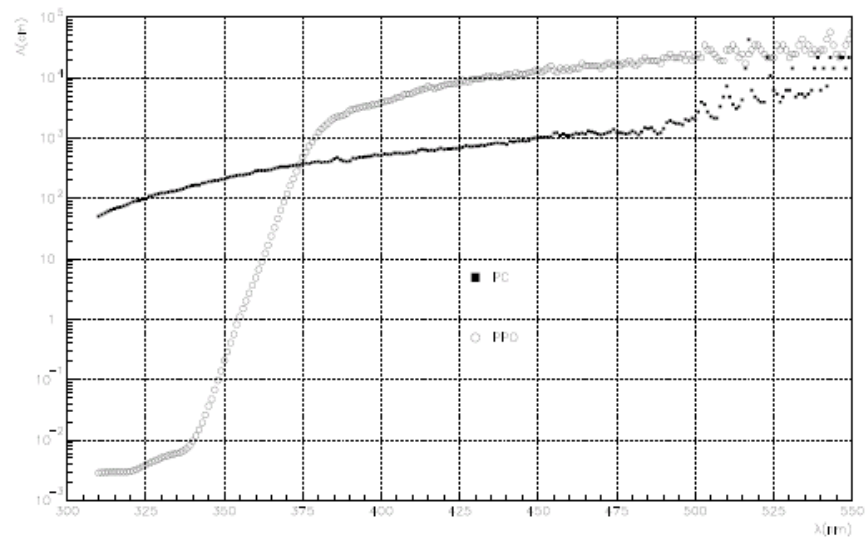


Fig. 7. Attenuation length of PC (full squares) and PPO (empty circles).

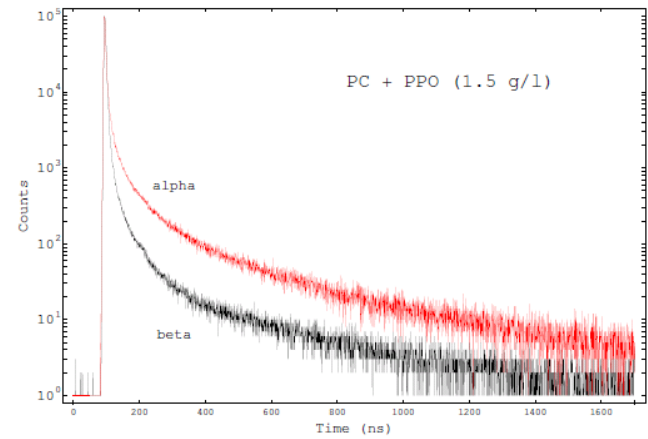


Fig. 8. Time response of the Borexino scintillator mixture for α and β particles.

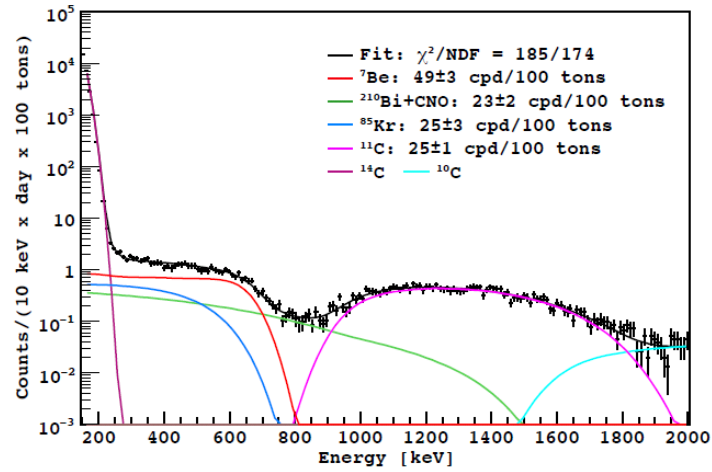


Figure 2. Spectral fit in the energy region 160–2000 keV. Contributions from ${}^{214}\text{Pb}$, pp , and pep neutrinos, not shown, are almost negligible with respect to those in the figure.